ISSN 0021-3640, JETP Letters, 2023, Vol. 117, No. 8, pp. 624–629. © The Author(s), 2023. This article is an open access publication.
Russian Text © The Author(s), 2023, published in Pis'ma v Zhurnal Eksperimental'noi i Teoreticheskoi Fiziki, 2023, Vol. 117, No. 8, pp. 626–631.

CONDENSED MATTER

Robust Ferrimagnetism in Quasi-Freestanding Graphene

A. G. Rybkin[a], * (ORCID: 0000-0002-8237-4959), A. V. Tarasov[a] (ORCID: 0000-0002-3628-4856), A. A. Gogina[a] (ORCID: 0000-0002-8577-8473), A. V. Eryzhenkov[a] (ORCID: 0000-0001-7560-5264), and A. A. Rybkina[a] (ORCID: 0000-0003-3215-1084)

[a] *St. Petersburg State University, St. Petersburg, 198504 Russia*

**e-mail: artem.rybkin@spbu.ru*

Received March 7, 2023; revised March 22, 2023; accepted March 22, 2023

The influence of the size of dislocation loops on sublattice ferrimagnetism in graphene is studied. It is shown that graphene and the underlying gold layer with Au/Co dislocation loops of various sizes are characterized by ferrimagnetic ordering within atomic layers. Additional gold adatoms under graphene enhance the induced Rashba spin–orbit coupling in graphene but do not destroy the ferrimagnetic order in graphene. Since gold clusters can remain during the intercalation of gold on the surface of graphene and under graphene, the number and size of clusters after intercalation can be controlled to enhance the induced Rashba interaction and to obtain a topological phase in graphene.

DOI: 10.1134/S0021364023600866

INTRODUCTION

The control of the spin structure in graphene, i.e., spin splitting of its electronic states and a topologically nontrivial band gap at the Dirac point, is one of the most important problems of materials science today, which should be solved in order to use graphene in spintronics, especially for the implementation of nondissipative transport. It is known that a strong spin–orbit coupling is a necessary condition for observing the quantum spin Hall effect [1], quantum anomalous Hall effect (QAHE) [2–4], and other effects. The second factor affecting the spin structure is the exchange interaction in graphene. In this regard, special attention is paid to theoretical and experimental studies of the possible magnetic order in superatomic graphene [5], twisted bilayer graphene [6], triangulene [7], nanographenes [8], and other two-dimensional carbon systems. The experimentally unimplemented Haldane model based on a graphene lattice with an inhomogeneous distribution of the magnetic field on the atomic scale [9] remains relevant and attractive, since it predicts the QAHE in a two-dimensional hexagonal lattice.

Of no small importance is the magnetic proximity effect, which is a promising way to implement the exchange splitting of electronic states [2, 10] without applying an external magnetic field, which can also be used to implement the QAHE, provided that the topological nontriviality of electronic states is preserved. Previously, it was shown that the contact of graphene with antiferromagnetic oxide can lead to the QAHE or the quantum valley Hall effect, depending on the direction of magnetization [11]. The authors of [12] reported on the implementation of magneto-spin–orbit graphene at the Au/Co(0001) interface with dislocation loops. The results of theoretical calculations have shown that the spin–orbit coupling and exchange interaction induced in graphene lead to the asymmetry of the spin splitting at opposite $\overline{K}$ and $\overline{K}'$ points. The intercalation of a smaller amount of gold under graphene made it possible to transfer from *p*-doped graphene to *n*-doped graphene with the shift of the Dirac point from the conduction band to the valence band [13]. It was shown that the synthesized graphene is characterized by ferrimagnetic ordering on the carbon atoms of two sublattices, usually referred to as A and B sublattices. Using the tight-binding model [4, 13], Berry curvatures opposite in sign were obtained at opposite $\overline{K}$ and $\overline{K}'$ points, which made it possible to propose *n*-doped graphene to implement the theoretically predicted circular dichroism Hall effect. However, until now, the giant Rashba effect with the spin–orbit splitting of π states near the Fermi level up to 100 meV was not confirmed in the density functional theory (DFT) calculations [13–16]. The origin of this discrepancy between theoretical and experimental results may be structural differences in the synthesized and model systems and the additional effect of phonon oscillations on the spin–orbit coupling [17, 18] in graphene.

In this work, we study the stability of the ferrimagnetic order on graphene sublattices at the Au/Co(0001) interface with respect to possible structural changes in a real system: the formation of dislocation loops of various sizes under graphene and the

appearance of additional cobalt and gold atoms near graphene. The need to study this issue is confirmed by the results obtained in [19], where the presence of nickel atoms on the surface alloy, which are displaced from the upper nickel atomic layer during alloying, is discussed, and the formation of dislocation loops of various sizes for the Au monolayer on Ni(111) is demonstrated. On the other hand, the surface phases with gold clusters under graphene and with residual gold clusters on the graphene surface after intercalation, which can affect the electronic structure of graphene, were reported in [20, 21]. Thus, the study of the role of structural differences between the synthesized and model systems is relevant.

ROLE OF DISLOCATION LOOPS IN THE FORMATION OF FERRIMAGNETISM IN GRAPHENE

Figure 1a shows the low-energy electron diffraction pattern with the ~(9 × 9) period of the superstructure. It is well known that monolayers of noble metals (Ag, Au) are alloyed with transition metals (Ni, Co, Cu) with the formation of triangular dislocation loops [12, 19, 22, 23]. The size of a single dislocation depends on the number of atoms displaced from the interface layer of the transition metal during its formation [19, 22]. It can be seen in Fig. 1b that dislocation loops formed under graphene are periodic over fairly large areas of the sample, but can have at least two dimensions: with three and six gold atoms constituting the side of the triangle (zero and six gold atoms at the center of the dislocation loop, respectively). As in [19], dislocation loops with six gold atoms in its central part are often found on the surface. Figures 1c and 1d show angle-resolved photoelectron spectroscopy (ARPES) intensity maps in the $\bar{\Gamma}\bar{K}$ direction of the surface Brillouin zone. A band gap E_g is observed in the electronic structure of the graphene Dirac cone. Theoretical calculations were carried out in order to study the electronic structure of graphene and to analyze the band gap value.

Density functional theory calculations of the electronic structure of the Gr/Au/Co(0001) system, which has a period of (9 × 9) and contains dislocation loops, showed that the self-consistent solution of the Kohn–Sham equation demonstrates a ferrimagnetic order on the A and B sublattices of graphene. The calculation results are presented in Fig. 2. During structural optimization, the nodal gold atoms in the dislocation are displaced closer to the cobalt layer, and their magnetic moments are codirectional with the magnetization of the cobalt layer. Most of the remaining gold atoms along the perimeter of the cell and on its right-hand side are magnetized against the magnetic moments of cobalt atoms. In a cell without a dislocation loop built on the basis of a structurally optimized cell with a dislocation loop with a Gr–Au distance of

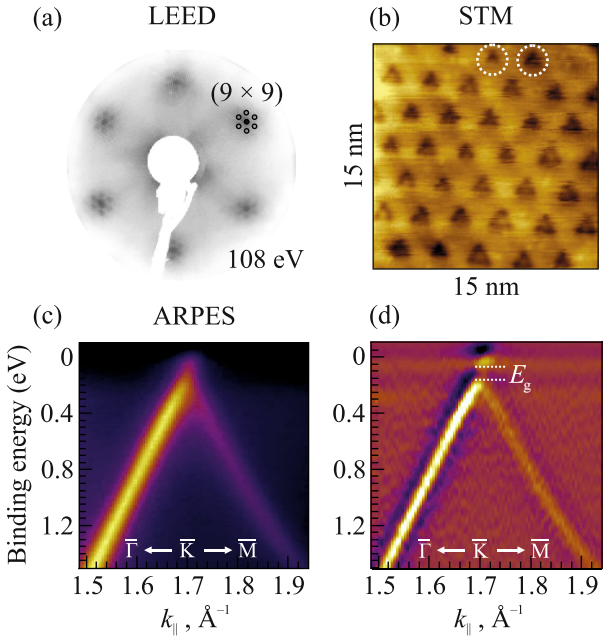

Fig. 1. (Color online) (a) Low-energy electron diffraction pattern of the Gr/Au/Co/W(110) system. (b) Scanning tunneling microscopy image of the surface. Dislocation loops of various sizes are marked by circles with dotted lines. (c) ARPES map in the $\bar{\Gamma}\bar{K}\bar{M}$ direction of the Brillouin zone and (d) its second energy derivative.

3.4 Å, no ferrimagnetic ordering is observed in the gold layer (Fig. 2c). In this case, all gold atoms have magnetic moments codirectional with those in the cobalt layer. Now, the consideration of the magnetic moments on atoms in graphene for the presented cells shows that the ferrimagnetic ordering in the graphene layer is present only in cells with dislocation loops (Fig. 2a). It can be seen in Fig. 2d that the ferrimagnetic ordering in graphene leads to a band gap at $\bar{K}$ points of graphene. On the contrary, for the cell without the dislocation loop, strong hybridization with the *d* states of cobalt is observed, and the band gap is no more than 30 meV. The theoretical results obtained are confirmed by angle-resolved and spin-resolved photoelectron spectroscopy data. According to these data, the band gap is (80 ± 25) meV (see Figs. 1c and 1d), and the spin splitting of π states is 40 and 80 meV near opposite $\bar{K}$ points with the magnetization of the cobalt layer in the surface plane and perpendicular to the $\bar{\Gamma}\bar{K}$ direction [13].

Thus, the (Au monolayer)/Co(0001) interface with periodic dislocation loops plays a key role in transferring the exchange interaction to graphene, since dislocations in the theoretical model radically change the picture of the electronic structure of graphene, creating a band gap in it caused by the electron–electron interaction according to the Hubbard model and nonequivalence of A and B sublattices.

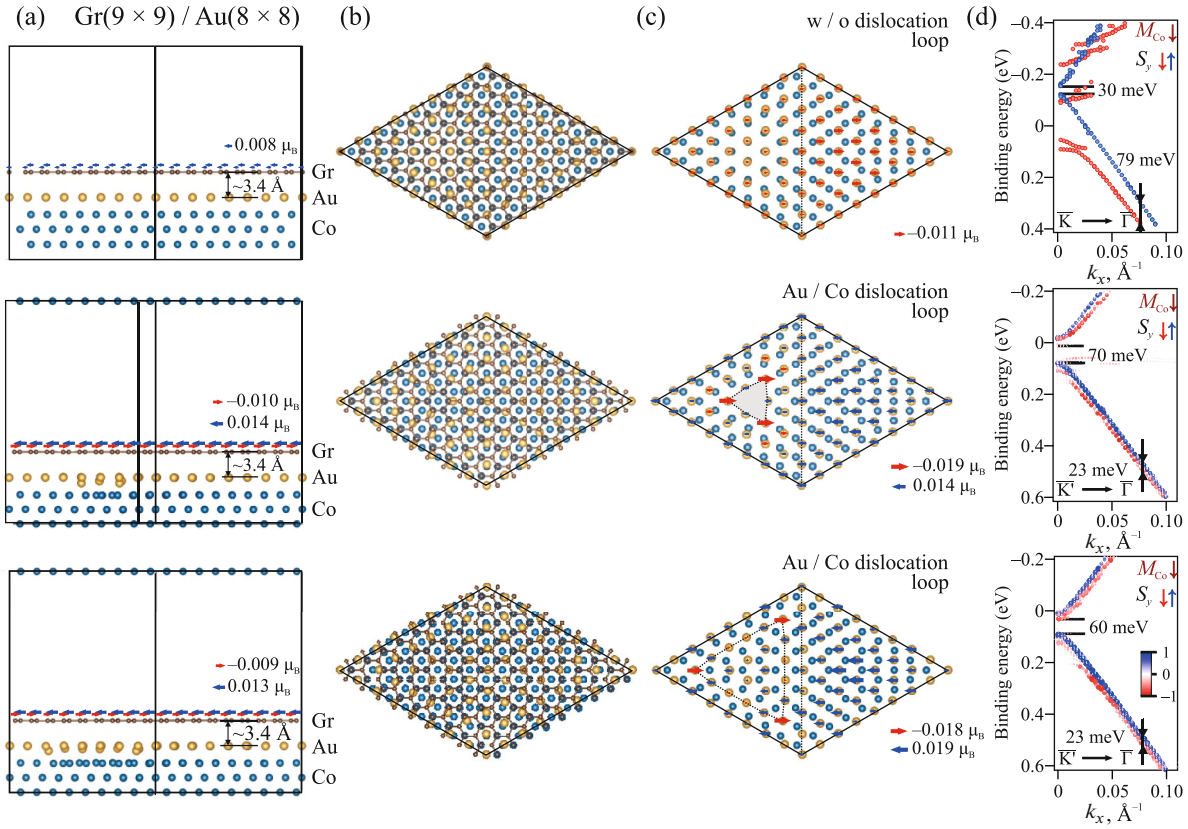

Fig. 2. (Color online) Unit cells of the Gr(9 × 9)/Au(8 × 8)/Co(0001) system without a dislocation loop and with dislocation loops of various dimensions: (a) side view, (b) top view, and (c) view of the Au–Co interface under graphene. (d) Corresponding unfolded (9 × 9) electronic structure near the $\bar{K}$ and $\bar{K}'$ points. The size and color of the symbols show the Bloch spectral weight for the S_y spin component.

INFLUENCE OF COBALT AND GOLD ADATOMS

To analyze the effect of possible structural inhomogeneities on the electronic and spin structure of graphene, DFT calculations were performed for the Gr/Au/Co system with different variants of additional atoms. We consider three main cases.

(i) A cluster of three cobalt atoms under graphene, which can be formed upon the formation of the smallest dislocation loop (see Fig. 3a). It can be seen in Fig. 3b that the π states of graphene (marked with a dotted line) are strongly hybridized with the *d* states of cobalt, and the Dirac cone is destroyed. At the same time, graphene is magnetized in a ferromagnetic manner with respect to the cobalt layer with magnetizations on carbon atoms of ~$0.9\mu_B$.

(ii) Gold adatoms under graphene as a result of excessive intercalation (see Fig. 3c). The electronic structure of graphene for this case is shown in Fig. 3d. It is found that ferrimagnetism is preserved for this system in a graphene lattice with magnetizations of ~$0.010–0.011\mu_B$ and $-(0.011–0.012)\mu_B$ on sublattices; an additional gold atom in the cell leads to an increase in the Rashba splitting in the region of the Dirac cone to ~20 meV. The band gap width is ~60 meV and is due to the antiferromagnetic interaction in graphene. It is noteworthy that the Rashba splitting in this case (~20 meV) is still less than the experimental value (~60 meV). The corrugation of the gold layer under graphene and the contribution of phonon vibrations of graphene can make a significant contribution to the giant Rashba splitting effect, which is the subject of further research.

(iii) Gold adatoms on graphene remaining on the surface after intercalation (see Fig. 3e). In this case, the Rashba splitting near the Fermi level does not increase, and it is less than 7 meV. In contrast to the previous case, there is no spin inversion with respect to the $\bar{\Gamma}$ point, indicating the prevailing contribution of exchange splitting, up to ~50 meV. In this case, the ferrimagnetic order is preserved, but the fraction of the antiferromagnetic interaction decreases, which leads to a decrease in the band gap at the Dirac point to 40 meV. A similar decrease in the fraction of antiferromagnetic ordering is observed for the case of graphene close to the gold layer by 0.3 Å from the equilibrium state.

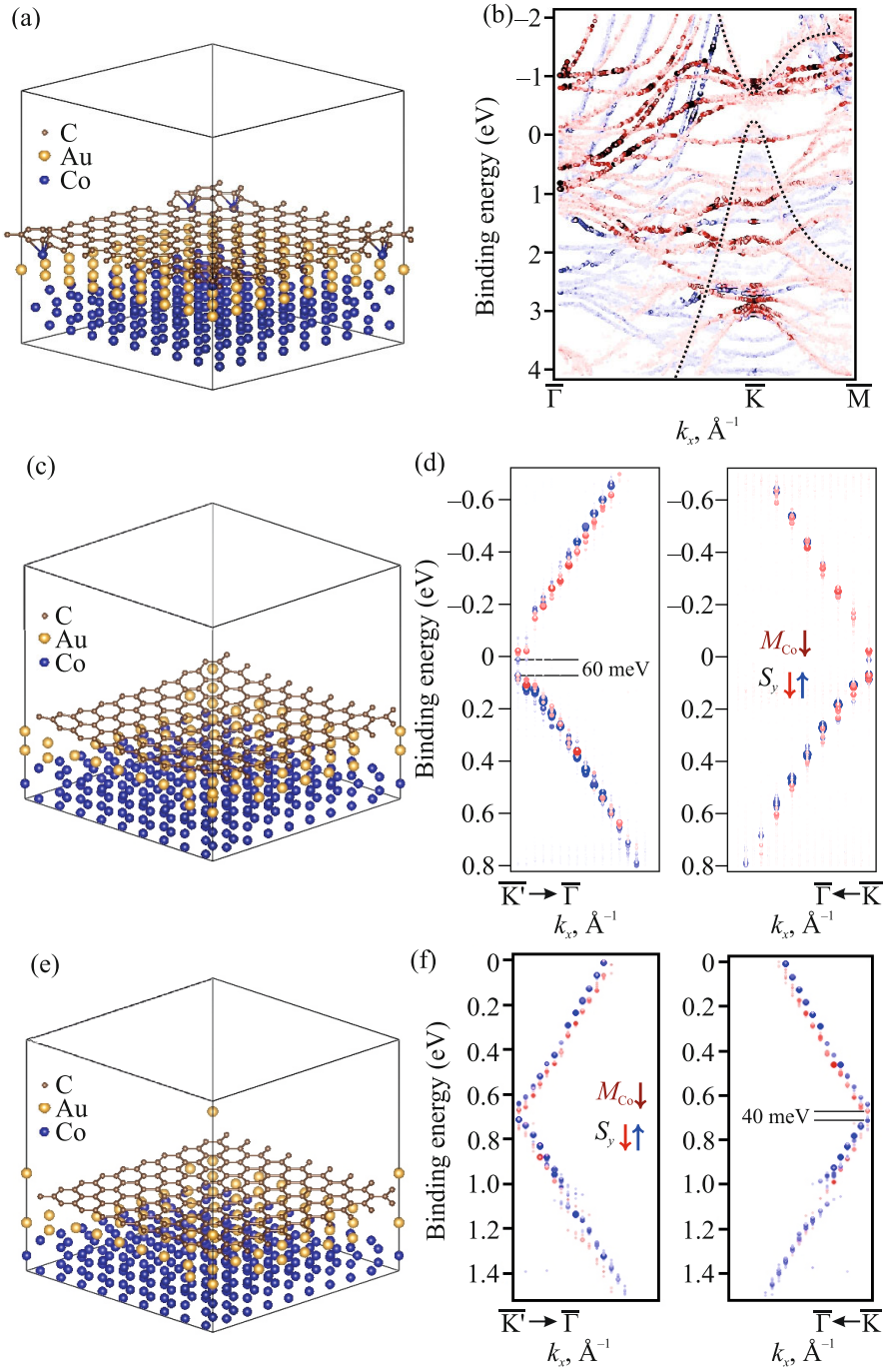

Fig. 3. (Color online) Unit cell with additional atoms: (a) cobalt under graphene, (c) gold under graphene, and (e) gold over graphene. (b, d, f) Unfolded electronic structure near the $\overline{K}$ and $\overline{K}'$ points corresponding to the unit cells shown on the left. The graphene π zone is marked by a dotted line in (b). The size and color of the symbols show the Bloch spectral weight for the S_y spin component.

CONCLUSIONS

The studies performed have indicated that graphene on Au/Co dislocation loops of various sizes is characterized by the ferrimagnetic ordering on its sublattices. Additional gold adatoms under graphene enhance the induced Rashba spin–orbit coupling in graphene, but do not destroy its ferrimagnetic ordering. Controlling the number of gold atoms above/below graphene can be used to find the optimal relation between spin–orbit coupling and exchange

interaction to observe the quantum anomalous Hall effect.

EXPERIMENTAL METHODS

Measurements were carried out at the unique scientific facility Nanolab at the Resource Center Physical Methods of Surface Investigation, Research Park, St. Petersburg State University. Epitaxial well-oriented graphene grown on Co(80 Å)/W(110) by chemical vapor deposition was intercalated with an Au monolayer after the deposition of 3.1 Å Au followed by annealing to 600°C. A synthesized sample was magnetized along the easy magnetization axis of a thin Co film (along the $-y$ axis in the plane of the surface perpendicular to the $\overline{\Gamma}\overline{\mathrm{K}}$ direction).

Ab initio DFT calculations were carried out at the Computing Center, Research Park, St. Petersburg State University. The full potential method of augmented plane waves + local orbitals [24], implemented in the WIEN2k code [25], was used with the generalized gradient approximation (GGA) in the Perdew–Burke–Ernzerhof (PBE) version [26]. The parameter $RMT \times K_{\max}$, where RMT is the smallest radius of an atomic sphere and $K_{\max}$ is the plane wave basis cutoff, which determines the accuracy of calculations, was 3.30 in all calculations performed. The radii of the atomic spheres were set equal to $1.35a_0$ for carbon, $2.46a_0$ for gold, and $2.18a_0$ for cobalt, where a_0 is the Bohr radius. The structure of the interfaces was simulated using periodic supercells in the approximation of periodic crystal slabs, consisting of four substrate layers (three layers of cobalt and one layer of gold) coated with graphene on one side, and a vacuum region extending for more than 20 Å. A discrete $1 \times 1 \times 1$ k grid of the Brillouin zone was chosen during the self-consistent field procedure. The positions of the atoms in each unit cell were relaxed within the scalar-relativistic approximation until the forces per atom became less than 1 mRy/a_0 ($\approx 3 \times 10^{-2}$ eV/Å). The spin–orbit coupling was taken into account by the second variation method with scalar-relativistic orbitals as basis functions [27]. The band structure of the supercell was unfolded according to the method described in [28].

ACKNOWLEDGMENTS

We are grateful to the Laboratory of the Electronic and Spin Structure of Nanosystems, St. Petersburg State University, and the Research Park, St. Petersburg State University, for their assistance in conducting research and using the equipment.

FUNDING

This study was supported by the Russian Science Foundation (project no. 23-22-00112, https://rscf.ru/project/23-22-00112/).

CONFLICT OF INTEREST

The authors declare that they have no conflicts of interest.

OPEN ACCESS

REFERENCES

1. C. L. Kane and E. J. Mele, Phys. Rev. Lett. **95**, 146802 (2005).
2. V. T. Phong, N. R. Walet, and F. Guinea, 2D Mater. **5**, 014004 (2017).
3. V. N. Men'shov, I. A. Shvets, and E. V. Chulkov, JETP Lett. **110**, 771 (2019).
4. A. Eryzhenkov, A. Tarasov, A. Shikin, and A. Rybkin, Symmetry **15**, 516 (2023).
5. Y. Zhou and F. Liu, Nano Lett. **21**, 230 (2021).
6. A. O. Sboychakov, A. V. Rozhkov, and A. L. Rakhmanov, JETP Lett. **116**, 729 (2022).
7. N. Pavliček, A. Mistry, Z. Majzik, N. Moll, G. Meyer, D. Fox, and L. Gross, Nat. Nanotech. **12**, 308 (2017).
8. S. Mishra, X. Yao, Q. Chen, K. Eimre, O. Gröning, R. Ortiz, M. Di Giovannantonio, J. C. Sancho-García, J. Fernández-Rossier, C. A. Pignedoli, K. Müllen, P. Ruffieux, A. Narita, and R. Fasel, Nat. Chem. **13**, 581 (2021).
9. F. D. M. Haldane, Phys. Rev. Lett. **61**, 2015 (1988).
10. D. N. Dresvyankin, A. V. Rozhkov, and A. O. Sboychakov, JETP Lett. **114**, 763 (2021).
11. H. Takenaka, S. Sandhoefner, A. A. Kovalev, and E. Y. Tsymbal, Phys. Rev. B **100**, 125156 (2019).
12. A. G. Rybkin, A. A. Rybkina, M. M. Otrokov, O. Y. Vilkov, I. I. Klimovskikh, A. E. Petukhov, M. V. Filianina, V. Y. Voroshnin, I. P. Rusinov, A. Ernst, A. Arnau, E. V. Chulkov, and A. M. Shikin, Nano Lett. **18**, 1564 (2018).
13. A. G. Rybkin, A. V. Tarasov, A. A. Rybkina, D. Yu. Usachov, A. E. Petukhov, A. V. Eryzhenkov, D. A. Pudikov, A. A. Gogina, I. I. Klimovskikh, G. di Santo,

L. Petaccia, A. Varykhalov, and A. M. Shikin, Phys. Rev. Lett. **129**, 226401 (2022).

14. J. Sławińska and J. I. Cerdá, Phys. Rev. B **98**, 075436 (2018).
15. E. Voloshina and Y. Dedkov, Adv. Theory Simul. **1**, 1800063 (2018).
16. J. Sławińska and J. I. Cerdá, New J. Phys. **21**, 073018 (2019).
17. B. Monserrat and D. Vanderbilt, arXiv: 1711.06274v1 (2017).
18. M. Schlipf and F. Giustino, Phys. Rev. Lett. **127**, 237601 (2021).
19. L. P. Nielsen, PhD Thesis (Univ. of Aarhus, Aarhus, 1995). https://phys.au.dk/fileadmin/site_files/publikationer/ phd/Lars_Pleth_Nielsen.pdf.
20. M. Krivenkov, E. Golias, D. Marchenko, J. Sánchez-Barriga, G. Bihlmayer, O. Rader, and A. Varykhalov, 2D Mater. **4**, 035010 (2017).
21. A. A. Rybkina, A. G. Rybkin, I. I. Klimovskikh, P. N. Skirdkov, K. A. Zvezdin, A. K. Zvezdin, and A. M. Shikin, Nanotechnology **31**, 165201 (2020).
22. J. Jacobsen, L. P. Nielsen, F. Besenbacher, I. Stensgaard, E. Lægsgaard, T. Rasmussen, K. W. Jacobsen, and J. K. Nørskov, Phys. Rev. Lett. **75**, 489 (1995).
23. A. Bendounan, H. Cercellier, Y. Fagot-Revurat, B. Kierren, V. Yu. Yurov, and D. Malterre, Phys. Rev. B **67**, 165412 (2003).
24. G. K. H. Madsen, P. Blaha, K. Schwarz, E. Sjöstedt, and L. Nordström, Phys. Rev. B **64**, 195134 (2001).
25. P. Blaha, K. Schwarz, G. K. H. Madsen, K. Dieter, J. Luitz, R. Laskowski, F. Tran, and L. D. Marks, *WIEN2k, An Augmented Plane Wave Plus Local Orbitals Program for Calculating Crystal Properties* (Vienna Univ. Technol., Austria, 2001).
26. J. P. Perdew, K. Burke, and M. Ernzerhof, Phys. Rev. Lett. **77**, 3865 (1996).
27. D. D. Koelling and B. N. Harmon, J. Phys. C: Solid State Phys. **10**, 3107 (1977).
28. O. Rubel, A. Bokhanchuk, S. J. Ahmed, and E. Assmann, Phys. Rev. B **90**, 115202 (2014).

Translated by L. Mosina